Experimental analysis of the feasibility of using the ground as a temporary energy accumulator

Andrés Meana-Fernández[a], María José Suárez-López[b], Eduardo Blanco[c], Jesús-Ignacio Prieto[d] and David García[e]

[a,b,e] Thermal Machines and Engines Area, Department of Energy, University of Oviedo, Gijón, Spain, e-mail: [a]andresmf@uniovi.es (CA), [b]suarezlmaria@uniovi.es, [e]garciamdavid@uniovi.es
[c] Fluid Mechanics Area, Department of Energy, University of Oviedo, Gijón, Spain, e-mail: eblanco@uniovi.es
[d] Applied Physics Area, Department of Physics, University of Oviedo, Oviedo, Spain, e-mail: jprieto@uniovi.es

Abstract:

With significant percentages of worldwide energy consumption occurring in the building sector, it is intended to reduce energy consumption and, in turn, satisfy the demand with renewable energies. However, renewable energies suffer from high variability, so energy accumulation systems become relevant for adjusting the time gap between energy supply and demand. In recent years, air conditioning facilities with geothermal heat pumps have been on the rise, as they reach higher coefficients of performance (COP) than aerothermal heat pumps. In addition, they provide the opportunity to use the ground as a thermal reservoir. A first analysis of the feasibility of using the ground as a temporary energy accumulator has been performed in this work. To this end, tests have been carried out in an experimental facility with vertical buried pipes to evaluate the evolution of ground temperature after heat injection. Temperature probes were placed on the pipe surface and monitored at 5 different depths, with tests performed in three different months to observe seasonal effects. Dimensional analysis led to the identification of the influencing variables of the problem: depth, tube length, tube diameter, time and soil thermal diffusivity. An apparent thermal diffusivity was defined to characterize the soil from the thermal measurements. The results allowed identifying a subterranean water stream at a particular depth, as well as observing the effects of ambient conditions in the system. It was observed that the upper ground layers were heavily affected by ambient conditions, discouraging their use for thermal energy storage, whereas depths below the ground water table seemed suitable for storing heat efficiently. Differences were found between wet and dry soil, with wet soil better suited for the storage of higher energy amounts, but dry soil better suited for keeping the stored energy for longer periods without further isolation.

Keywords:

thermal energy storage; thermal reservoir; energy supply; temporary energy accumulator; experimental testing.

1. Introduction

Almost half of global energy use is employed for heat generation purposes, being the building sector one of the highest contributors to global emissions. In the current energy and environmental context, both the reduction of energy consumption and the use of renewable energy sources are critical issues. When renewable energy sources are used, the availability of energy often does not coincide with its need [1], so an accumulation system is interesting to absorb the gap between energy production and demand [2].

Among renewable energies, geothermal energy has been widely used from prehistoric times to the present day [3]. As the ground temperature keeps more constant along the year than the ambient temperature, it is very interesting for heating and cooling applications in buildings. This feature, combined with high COP heat pumps consists of a reliable solution itself. Furthermore, the geothermal facility can be used to store surplus production by other renewable sources, as it is the case of solar thermal projects [4,5]. Although ground has usually been used for long term accumulation purposes [6,7], Cruickshank and Baldwin [8] studied the diurnal performance, showing the interest in using the ground not only for long term accumulation purposes.

In the first decade of this century, five “Office Buildings Prototypes for Research and Demonstration” were constructed or retrofitted within the Singular Strategic Project ARFRISOL [9], showing the construction of more environmentally respectful buildings. As a complement to that project, the Gijón Solar Cooling Laboratory (GSCL) [10] was installed at the University of Oviedo. The GSCL is a modular plant that allows the testing of diverse equipment and technologies, including a geothermal installation with vertical buried pipes. With the fundings of the project RehabilitaGeoSol [11] the experimental equipment was completed, and the first test of the vertical pipes circuit has been obtained.

https://doi.org/10.52202/069564-0188

In this work, experimental results obtained during months of testing in the vertical buried pipes of the GSCL are analysed, and first impressions on the influence of the season on the thermal behaviour of the soil are discussed.

2. Materials and methods

2.1. Description of the vertical pipes circuit

The GSCL was designed and implemented for testing different technologies for solar cooling production in buildings. The laboratory is in the facilities that the University of Oviedo has in the Gijon Polytechnical Engineering School. The core of this facility is an absorption machine ClimateWell-CW10, connected to several heat sources and sinks. The absorption machine has two different barrels of lithium chloride and water, enabling the possibility of storing energy in one of the barrels while the other one is discharging. The heat dissipation from the absorption machine can be configured through different technologies: an air heat exchanger, an evaporative cooling tower, a water reservoir or different ground heat exchangers with horizontal or vertical buried pipes. Figure 1 shows the conceptual scheme of the vertical pipes circuit tested in this paper.

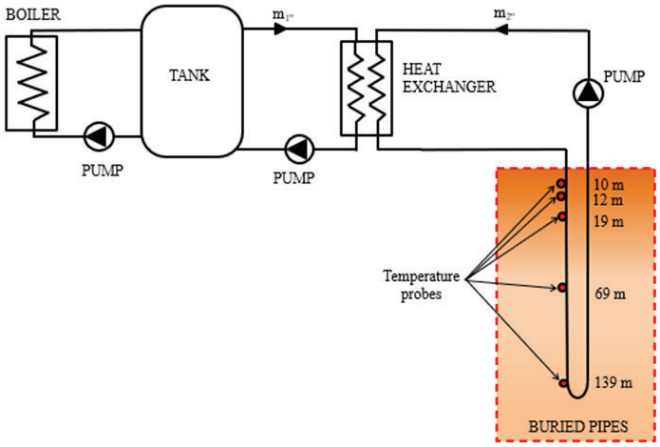

Figure 1. Conceptual scheme of the vertical pipes circuit.

The vertical pipes circuit consists of 2 U circuits of 32 mm diameter pipes, placed together into a 140 mm diameter hole filled with gravel, as can be seen in Figure 2. The pipes are buried down to 140 m depth, and 3-wires PT-100 probes are fitted to the outer surface of the pipes at five different depths (10 m, 12 m, 19 m, 69 m and 139 m), whereas flowrates were monitored with Kobold inductive flowmeters. PT-100 probes and flowmeters are connected to a Keithley 2700, multimeter equipped with a Keithley 7700 acquisition board and a GPIB/USB interface to be connected to a PC which records data every 5 minutes.

Figure 2. Detail of the pipes entering the ground.

2.2. Variables influencing in the problem

As a first approximation to the complexity of the problem, the temperature and physical properties of the terrain are assumed to be scalar functions with cylindrical symmetry. It is also assumed that the thermal conductivity of the terrain is isotropic. On the other hand, pending evaluation of the possible influence of environmental conditions by experimental results, the ground surface is assumed to be adiabatic.

At a point in the ground at distance r from the pipes and depth z from the surface, the temperature difference ΔT with respect to a point at the same depth and away from the influence of the pipes, depends on the physical properties of the ground, namely thermal conductivity k, specific heat capacity c and density ρ, the

https://doi.org/10.52202/069564-0188

diameter D and length L of the pipes, the temperature difference ΔT_0 at the beginning of the cooling, and the elapsed cooling time t. Therefore, a functional relationship of the following type can be written:

$$\Delta T = f(r, z, D, L, k, \rho, c, \Delta T_0, t) \quad (1)$$

The application of Buckingham's pi theorem to this equation, with the classical dimensional basis $\{L, M, T, \theta\}$ and using L, ρ, c and ΔT_0 as reference quantities, leads to the following functional relationship between dimensionless groups:

$$\frac{\Delta T}{\Delta T_0} = F\left(\frac{r}{L}, \frac{z}{L}, \frac{D}{L}, \Pi_k, \Pi_t\right) \quad (2)$$

where $\Pi_k = k/\left(\Delta T_0^{1/2} \rho\, L\, c^{3/2}\right)$ and $\Pi_t = \Delta T_0^{1/2} c^{1/2}\, t/L$.

Since the product of Π_k and Π_t is equal to the Fourier number $Fo = \alpha t/L^2$, equation (2) can be rewritten as follows:

$$\frac{\Delta T}{\Delta T_0} = F\left(\frac{r}{L}, \frac{z}{L}, \frac{D}{L}, Fo, \Pi_t\right) \quad (3)$$

The influence of Π_t is neither theoretically nor experimentally justified in the literature applicable to similar problems. In Appendix A it can be seen that spatially discriminated dimensional analysis predicts that such a monomial is spurious. Furthermore, variables r, D and L are constants in the case study, so the following functional relationship can be proposed as the basis of the experimental analysis:

$$\frac{\Delta T}{\Delta T_0} = F\left(\frac{z}{L}, Fo\right) \quad (4)$$

2.3. Data curation and postprocessing

The tests performed may be divided into two stages, as depicted in the example of Figure 3. In the first stage, heat was injected into the geothermal circuit below the ground until stationary conditions were obtained. After that, the heat supply was cut off and the evolution of the system was monitored. Specifically, the evolution of the temperature probes placed on the tube walls at 10, 12, 19, 69, and 139 m of depth was measured, and at first sight no influence of ambient temperature oscillations was found, even at the lower depth probes. The summary of the experimental tests performed is collected in Table 1. The tests were performed in May and September 2019 and February 2020, to observe seasonal effects in the behavior of the system.

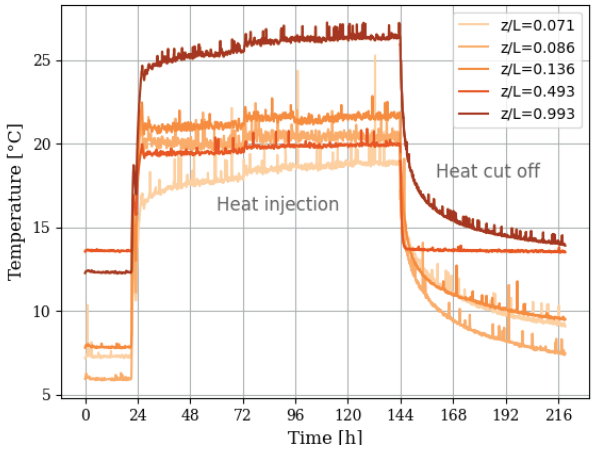

Figure 3. Loading curves performed in the experiments of May 2019.

Table 1. Summary of experimental tests

	February	May	September
Heat injection time	10,110 min	8,685 min	20,000 min
Heat injection flowrate	11.6 L/min	19.2 L/min	22.5 L/min
Average heat injection power	14 kW	17.5 kW	15.5 kW
Heat cut off monitoring time	21,690 min	4,515 min	19,315 min
Total experiment time	31,800 min	13,200 min	39,315 min

The measurements obtained were firstly filtered with a third order one-dimensional median filter [12] to eliminate possible outliers and obtain a clean signal for its subsequent analysis. An example is shown in Figure 4 for illustration.

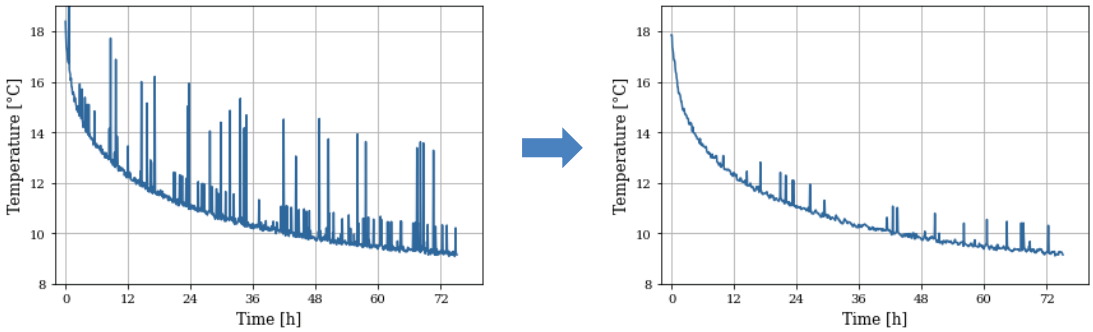

Figure 4. Postprocessing of measurements with 3rd order 1-D median filter

Then, the data were made dimensionless to compare measurements from different depths and periods. As the exact thermophysical properties of the soil are unknown, a constant apparent thermal diffusivity $\alpha_{ref} = 5.288 \cdot 10^{-7}$ m²/s was firstly used to make the data dimensionless. This value was estimated from the values obtained in the RehabilitaGeosol project [11] for the area of the experiments: a density of 3200 kg/m³, a specific heat of 1300 J/(kg·K), and a thermal conductivity of 2.2 W/(m·K). Thermal diffusivity was considered constant, and the underground soil isotropic.

It is possible, though, that each ground layer has different thermophysical properties. Therefore, with the aim of obtaining an estimative characterization of each ground layer, different apparent thermal diffusivities α_a were allowed for each ground depth (i.e., data series). The estimations of apparent thermal diffusivity α_a were obtained from the fitting of temperature measurements with respect to time. As a first approximation, in this work, an equation based on the proposed in [13] for transient heat conduction in semi-infinite solids was used, considering the soil as such:

$$\Delta T(t) = \Delta T_0 \operatorname{erf}\left(d/\sqrt{4\alpha_a t}\right) \quad (5)$$

Where T_0 is the initial temperature in K, T_∞ is the steady-state temperature in K, d is the distance between the tube center and the probe position, 0.07 m, α_a is the apparent thermal diffusivity of the soil in m²/s and t is the time in s. Typical values for soil thermal diffusivity are in the range of $5 \cdot 10^{-7}$ m²/s, [14,15,16] so values of α_a in the order of magnitude of 10^{-7} are expected.

2.4. Influence of ambient conditions

The soil is constituted by different minerals and rocks of different sizes, leaving gaps in between that may be filled with liquids and gases [17]. The estimation of soil thermophysical properties becomes a challenge due to this heterogeneous composition of the soil, which affects density, thermal conductivity, heat capacity and thus thermal diffusivity. When air is displaced by water from the gaps between solid fractions, the soil thermal conductivity is bound to increase. The increase of moisture also increases thermal conductivity due to the changes in the bond between water and soil, as well as the peculiar characteristics of water interfaces [18]. Volumetric heat capacity also increases with the addition of water. Once the thermal conductivity reaches a maximum value, the addition of more water continues increasing the soil heat capacity. As a consequence, thermal diffusivity exhibits an increasing trend for the addition of water at low moisture values, reaching a maximum for a particular moisture content, and then decreasing with further addition of water [19,20]. Apart from the composition, soil temperature affects its properties. Heat capacity and thermal conductivity are lower at lower temperatures, leading to variations in the thermal diffusivity of soil depending on the relative rate of change between these two variables.

In addition, it has been verified that ambient conditions influence the behavior of the upper ground layers and that both temperature and the amount of moisture influence soil properties [17], so meteorological data from the period in which the experiments were performed were collected from the Spanish State Agency for Meteorology [21] to provide a better insight into the results and their implications. Figure 5 shows the temperature and precipitation conditions at ground level from a month before starting the experiments until the experiments were finished. The exact dates in which the heat injection and cutoff processes for the experiment took place have been highlighted in the graphs. These data should help to generate the

https://doi.org/10.52202/069564-0188

landscape for understanding the initial conditions for the experiments and the evolution of the system throughout the heat injection and heat cutoff processes.

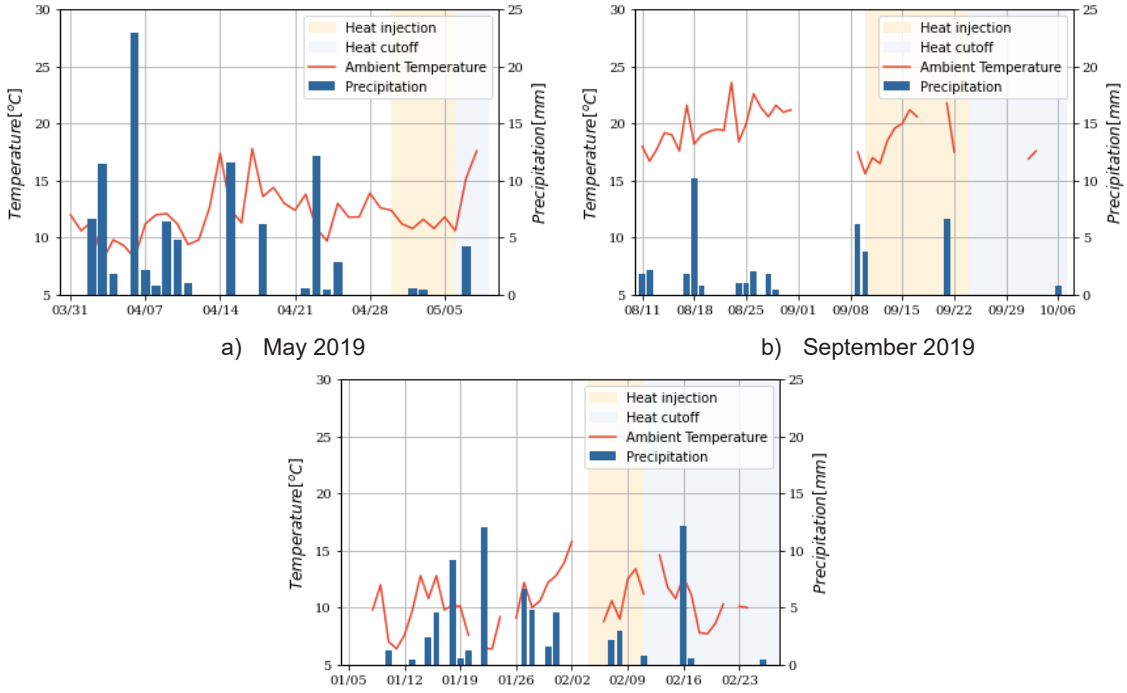

a) May 2019

b) September 2019

c) February 2020

Figure 5. Climate conditions above ground level at the experiment dates

Regarding the measurements from the meteorological station, it may be appreciated that there was a high period of rain before the experiments in May took place, with 91.9 mm, followed by February, with 49.2 mm and September, with 29.2 mm. Nevertheless, during the experiments, May had the driest conditions, 5.2 mm, followed by September, with 11.2 mm and February with 19.2 mm. Average temperatures are almost constant in the case of February, showing an increasing trend in May and a decreasing trend in September. Particularly, during the experiments, average ambient temperatures were 12.4 ºC in May, 18.4 ºC in September, and 10.7 ºC in February.

3. Results

3.1. Influence of depth

Figure 6 shows the evolution of dimensionless temperatures at all measured depths for the three seasons studied. It may be observed that there is an upper zone ($z/L \leq 0.086$), the temperature evolution is slower than in the lower zone ($z/L \leq 0.136$). This effect could be attributed to the fact that the water table where the experiments were performed is at 15 m underground ($z/L \leq 0.107$), so this depth could mark the fringe between both behavior types. A very different behavior may be appreciated for the temperatures at $z/L = 0.493$, which decrease abruptly as soon as heat injection is stopped. This behavior might be representative of a subterranean water stream, that draws heat at a higher rate than underground soil, as a result of the combination of conduction and also convection mechanisms. Comparing the three periods, the size of the gap between the upper and lower zones of the ground seems bigger in the case of May 2019. This could be attributed to the drier ambient conditions during the experiments, as the introduction of rainwater during the experiments in September and February may have helped to increase the slope of the cooling curves in these periods.

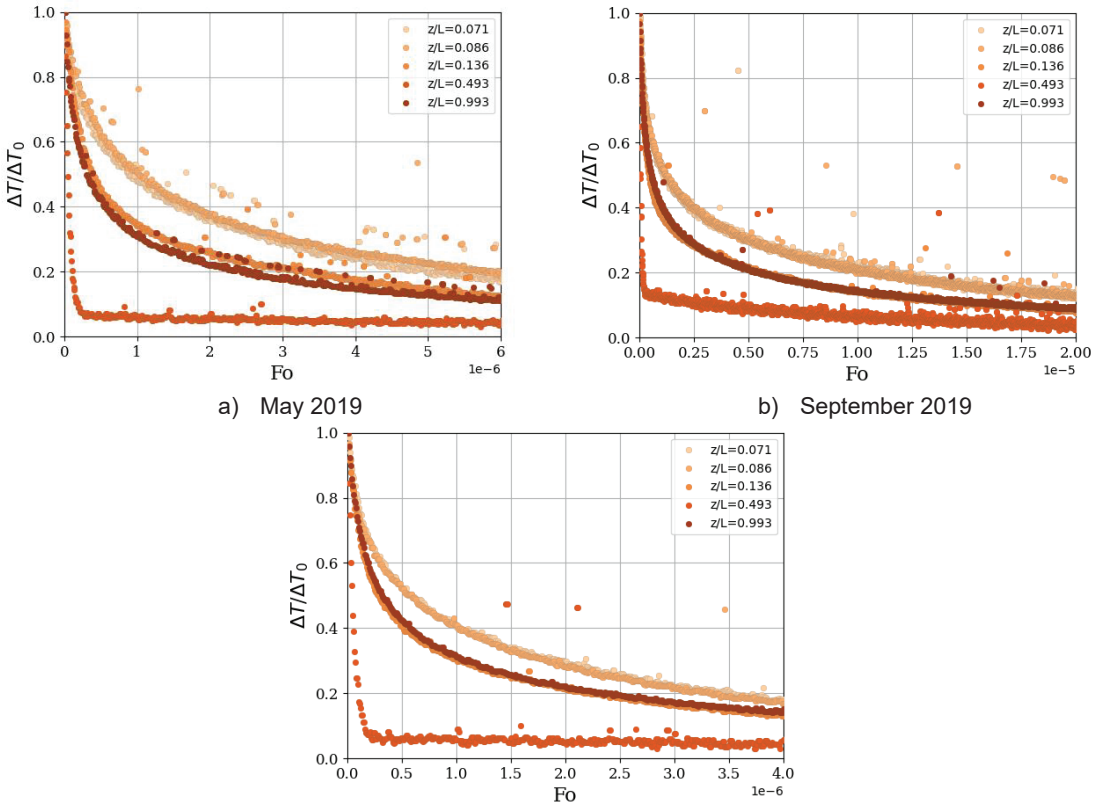

Figure 6. Evolution of dimensionless temperatures in different seasons (same layer diffusivities)

When different apparent thermal diffusivities were allowed for each ground depth, an interesting result was obtained: all curves, apart from the one with the alleged underground stream, collapsed into one in the dimensionless representation, as shown in Figure 7. This might suggest that the heat transfer physical mechanism could be the same for the collapsing curves, considering the different initial conditions and soil thermophysical properties. The results also lead to think that the physical mechanism of heat transfer at the specific depth z/L = 0.493 could be different from the others, so the presence of a subterranean water stream drawing heat by convection seems more feasible. In addition, different behaviors for the whole system arise in different seasons. The values of the apparent thermal diffusivity obtained for each season and depth have been collected in Table 3.

Table 3. Apparent thermal diffusivities as a function of dimensionless depth and season

	May	September	February
z/L	$\alpha \times 10^7$ [m²/s]	$\alpha \times 10^7$ [m²/s]	$\alpha \times 10^7$ [m²/s]
0.071	1.75	1.10	2.69
0.086	1.52	1.10	2.83
0.136	3.54	2.45	4.95
0.493	64.97	25.53	69.15
0.993	5.52	1.74	8.50

https://doi.org/10.52202/069564-0188

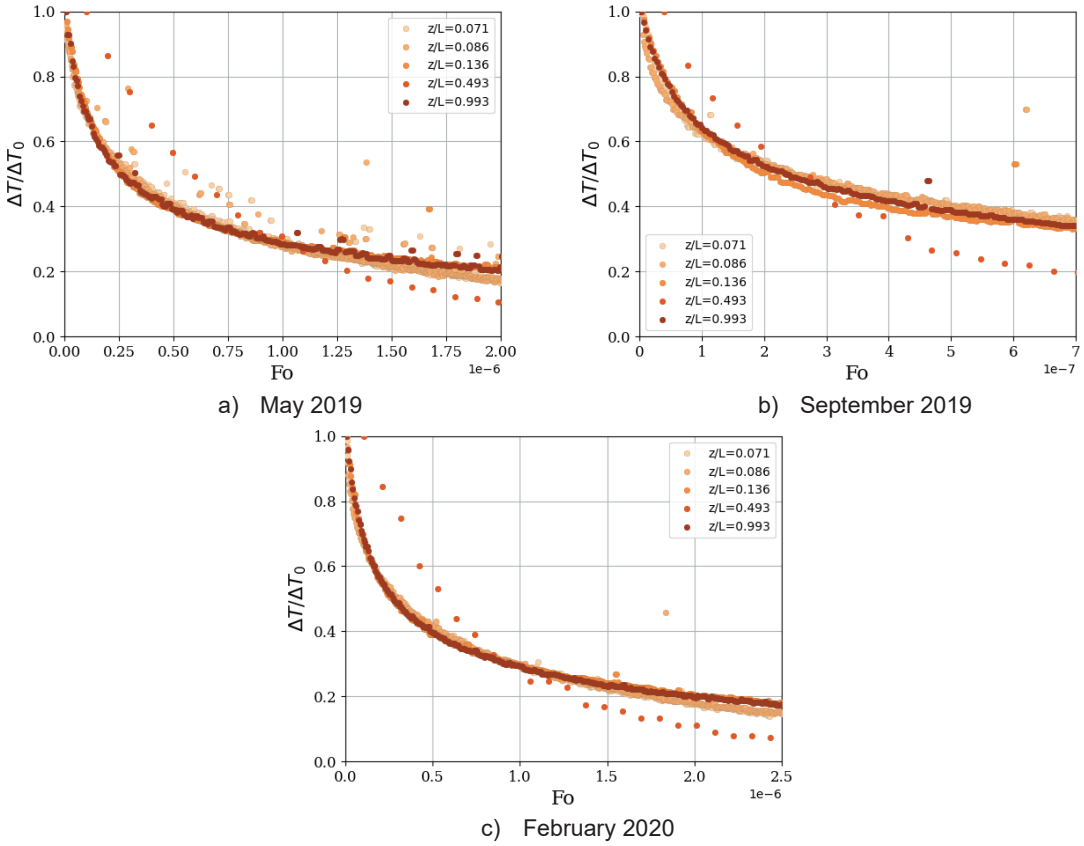

Figure 7. Evolution of dimensionless temperatures in different seasons (different layer diffusivities)

Note that for z/L = 0.493, apparent thermal diffusivity is much higher than for water, air, and typical soil values; this could be a last hint that there might be an underground water stream carrying heat away from the ground by convection, also affecting heat conduction speeds in the nearest ground layers.

3.2. Influence of seasons

Due to the differences observed between different seasons, the results of the temperature evolution at different depths as a function of the season were studied, as shown in Figure 8. February was found to be the season in which temperatures were lower. This difference, which is more apparent in the upper layers of the ground, may be ascribed to the fact that the air in contact with the ground surface is colder in that month, as seen in the meteorological data. In addition, during winter season, the ground temperature profile is near its minimum values. On the other hand, higher target ground temperatures are found in May and September, because of higher ambient temperatures. In May, the ground is getting warmer each day, as spring advances towards the summer, whereas in September, before the summer ends, the ground is still relatively warm. In addition, as seen in the climate data presented in Figure 5, more rain intensity was found in February and May, leading to possibly more drenched ground layers in which water displaces air from the soil pores, resulting in potentially higher thermal diffusivities. From this analysis, it seems that the energy potentially stored at such small depths would be very influenced by ambient conditions and could be easily dissipated, so it would not be recommended to store energy above the water table of the ground, unless adequate isolation systems are provided.

At higher depths, nevertheless, there is almost no difference between the temperature evolution in February and May. It seems reasonable to think that the effect of ambient temperature and the humidity caused by the rain stops having an influence at such depths. The difference between the behavior at such depths in September with respect to the other months may be ascribed to the higher temperatures reached at steady conditions in the ground, but a probably more reasonable explanation could be the less amount of water carried by the underground stream that certainly circulates near z/L = 0.493. The amount of water carried by this stream depends ultimately on the amount of rain, which is definitely lower towards the end of summer (see Figure 5), reducing the capability of the stream to cool the ground by convection.

https://doi.org/10.52202/069564-0188

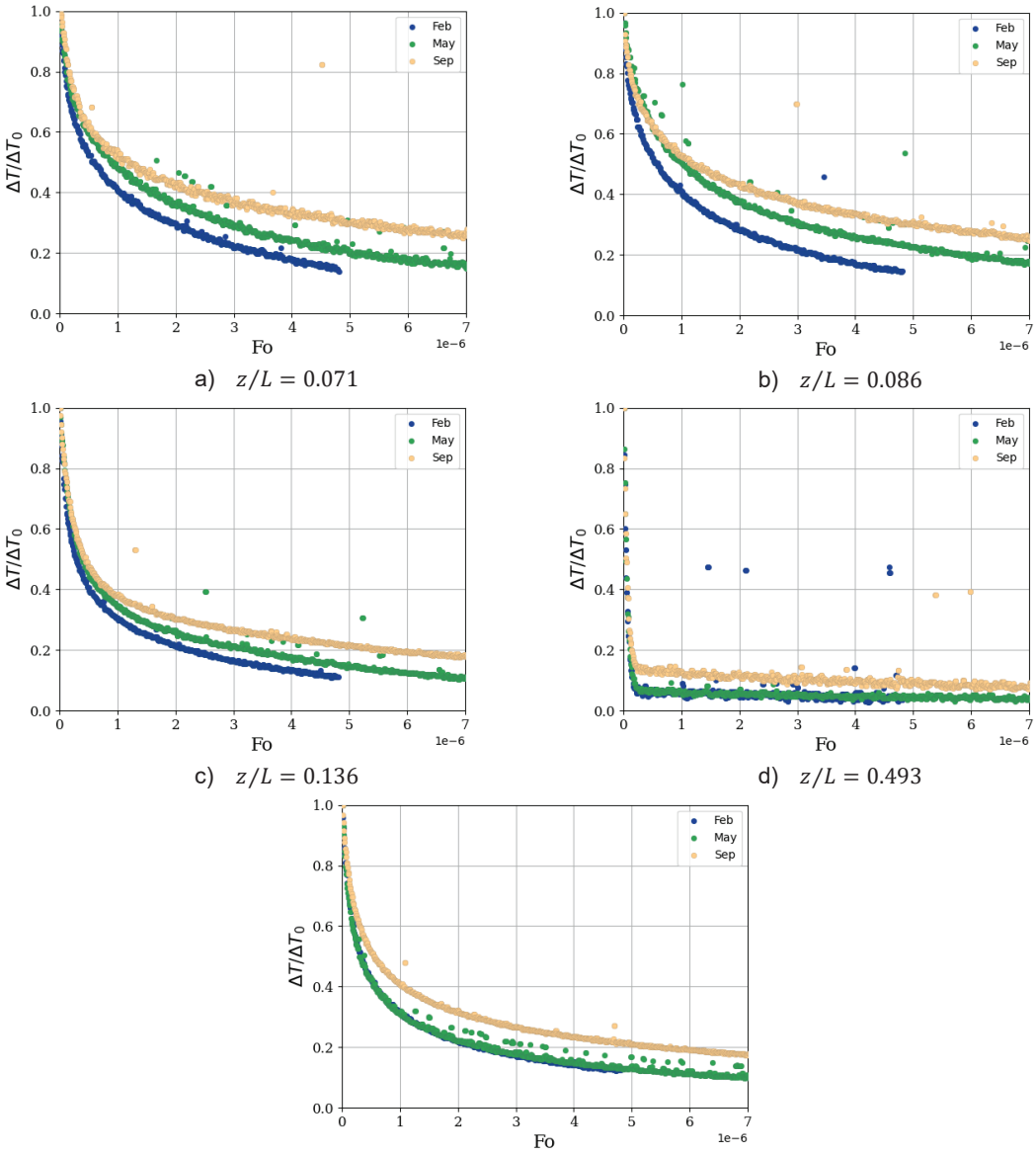

Figure 8. Evolution of dimensionless temperatures in different seasons at different depths

To summarize, wet soil tends to have a higher apparent thermal diffusivity up to a certain amount of moisture, allowing for faster loading and unloading curves for energy storage. Dry soil, on the other hand, needs more time for storing and releasing heat. This may be appreciated in the heat injection times depicted in Figure 5 for the drier seasons, and the higher Fourier numbers necessary to bring the soil back to its original temperature presented in Figure 6, which were substantially higher in September, when the soil was drier. Depending on the application and the required heating power, wet soil might represent an advantage for storing a higher amount of thermal energy and delivering it at higher speeds, thanks to the higher thermal diffusivity and specific heat. Isolating materials might help to keep the heat stored for longer times if seasonal storage is planned. Nevertheless, if heat delivery speed is not a limiting factor, dry soil should be able to keep heat stored during longer times, preventing its diffusion throughout the ground, without additional works for isolation.

4. Conclusions

A preliminary analysis of the feasibility of using the ground as a temporary energy accumulator has been performed in this work. To this end, experimental tests have been carried out with vertical buried pipes in the

https://doi.org/10.52202/069564-0188

Gijón Solar Cooling Laboratory (GSCL) facility, monitoring the temperature evolution of probes placed at different depths. The methodology proposed in this work may be used to characterize the ground thermal behavior and its feasibility as a temporary energy accumulator. Particularly, the soil composition, soil moisture and the presence of underwater currents have been found as variables of interest influencing the possible design and operation of storage systems.

Experimental measurements were represented against the dimensionless depth and the Fourier number, finding that depth has a significant influence in the evolution of temperatures, with differences between the behavior at the upper and lower layers of the ground, probably as a consequence of the water table depth.

In the upper zone, temperature evolutions were relatively slower than in the lower zones. A very different behavior was observed at z/L = 0.493, where heat was dissipated at a much higher speed, hinting at a different physical heat transfer mechanism, such as a subterranean water stream dissipating heat by convection. The numerical results presented in this work must be interpreted in a qualitative way, allowing the comparison between different measurements, but they must not be considered as an exact characterization of the thermophysical properties of the soil.

Different behaviors for the whole system were found depending on the season. An explanation may be provided by the different thermal conductivity values of water and air, which fill ground pores. A relationship between the meteorological historical data for temperature and precipitation and the behavior of the upper layers of the ground might be inferred with colder air leading to colder target values for the temperature and higher rain levels related to higher soil thermal conductivity and diffusivity values. Ambient conditions seemed to influence the system behavior at low depths, discouraging their use as a heat reservoir. However, at higher depths, ambient conditions did not show such a high influence, with practically the same behavior in February and May. There were, indeed, differences with September, but they are likely more related to the effects of a lower water mass flow at higher temperatures in the subterranean stream than the seasonal change in the soil conditions. Hence, heat storage at higher depths may be more reliable. Regarding soil moisture, wet soil might represent an advantage for storing a higher amount of thermal energy and delivering it at higher speeds, thanks to the higher thermal diffusivity and specific heat. Nevertheless, if heat delivery speed is not a limiting factor, dry soil should be able to keep heat stored during longer times. Finally, considering the impracticability of a total characterization of the soil characteristics, including pore geometry, along all the ground to be used as storage, heat loading and cutoff curves as the ones presented in this work may prove useful to assess the feasibility of using the ground as a temporary energy accumulator.

Future works will focus on the development and application of accurate models for heat transfer in buried U-vertical pipes to improve the characterization of the thermophysical properties of the ground, the study of the heat injection stage, and the development of more experimental tests at other ambient conditions to try to obtain more generalizable results.

Acknowledgments

This research was funded by the National Research and Development Plan 2004–2007 (Ref. PS-120000-2005-1), co-financed by ERDF funds and supported by the Spanish Ministry of Science and Innovation. This research has also been developed in the framework of the REHABILITAGEOSOL (RTC-2016-5004-3) project. It is a multidisciplinary R&D program supported by the Spanish Ministry of Science and Innovation and co-financed by European Regional Development Funds (ERDF). The authors would like to thank the AEMET OpenData system from the Spanish State Agency for Meteorology (AEMET), for making available the meteorological data used in this work.

Appendix A

The classical method of dimensional analysis does not take into account the algebraic characteristics of the influencing variables in a physical problem. The first references to the idea of considering differences between spatial dimensions are attributed to Williams [22] and Huntley [23]. Later, Palacios [24] deals rigorously with this topic and lays the foundations of discriminated dimensional analysis (DDA). There are recent examples of the use of the DDA method for various applications [25,26]. Spatial discrimination increases the order of the dimensional basis so that, in general, spurious dimensionless groups that might occasionally be deduced from the classical method are eliminated.

Using the DDA method, only the scalar variables in equation (1) have equal dimensional exponents in each of the three spatial directions. The dimensional formula for the thermal conductivity is derived from Fourier's Law and the definition of the heat flux Q:

$$\vec{q} = -\overline{\overline{k}} \otimes \nabla T \quad \text{(A.1)}$$

$$Q = \int \vec{q} \cdot \overrightarrow{\mathrm{d}S} \quad \text{(A.2)}$$

Using cylindrical coordinates and the dimensional basis $\{L_r, L_\varphi, L_z, M, T, \theta\}$ (Figure A1), the following equations can be written:

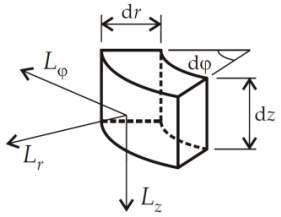

Figure A1. Spatial discrimination for Dimensional Analysis.

$$\vec{\dot{q}} = \begin{bmatrix} k_{rr} & k_{r\varphi} & k_{rz} \\ k_{\varphi r} & k_{\varphi\varphi} & k_{\varphi z} \\ k_{zr} & k_{z\varphi} & k_{zz} \end{bmatrix} \begin{bmatrix} \partial T/\partial r \\ \partial T/(r\partial\varphi) \\ \partial T/\partial z \end{bmatrix} \quad (A.3)$$

$$\dot{q}_r = k_{rr}\,\partial T/\partial r + k_{rz}\,\partial T/\partial z \quad (A.4)$$

$$\dot{q}_z = k_{zr}\,\partial T/\partial r + k_{zz}\,\partial T/\partial z \quad (A.5)$$

where it has been assumed that the temperature has cylindrical symmetry, i.e.: $T = T(r,z) \leftrightarrow \partial T/\partial\varphi = 0$

Therefore, the following dimensional formulae for the components of the thermal conductivity tensor are derived:

$$[k_{rr}] = \frac{[\dot{q}_r]}{[\partial T/\partial r]} = \frac{\left(L_r^{2/3}L_\varphi^{2/3}L_z^{2/3}MT^{-2}\right)/(TL_\varphi L_z)}{L_r^{-1}\theta} = L_r^{5/3}L_\varphi^{-1/3}L_z^{-1/3}MT^{-3}\theta^{-1} \quad (A.6)$$

$$[k_{rz}] = \frac{[\dot{q}_r]}{[\partial T/\partial z]} = \frac{\left(L_r^{2/3}L_\varphi^{2/3}L_z^{2/3}MT^{-2}\right)/(TL_\varphi L_z)}{L_z^{-1}\theta} = L_r^{2/3}L_\varphi^{-1/3}L_z^{2/3}MT^{-3}\theta^{-1} \quad (A.7)$$

$$[k_{zr}] = \frac{[\dot{q}_z]}{[\partial T/\partial r]} = \frac{\left(L_r^{2/3}L_\varphi^{2/3}L_z^{2/3}MT^{-2}\right)/(TL_r L_\varphi)}{L_r^{-1}\theta} = L_r^{2/3}L_\varphi^{-1/3}L_z^{2/3}MT^{-3}\theta^{-1} = [k_{rz}] \quad (A.8)$$

$$[k_{zz}] = \frac{[\dot{q}_z]}{[\partial T/\partial z]} = \frac{\left(L_r^{2/3}L_\varphi^{2/3}L_z^{2/3}MT^{-2}\right)/(TL_r L_\varphi)}{L_z^{-1}\theta} = L_r^{-1/3}L_\varphi^{-1/3}L_z^{5/3}MT^{-3}\theta^{-1} \quad (A.9)$$

As a result, the following matrix of dimensional exponents is obtained:

	r	D	z	L	ρ	c	k_{rr}	k_{rz}	k_{zz}	ΔT_0	t	ΔT
L_r	1	1	0	0	-1	2/3	5/3	2/3	-1/3	0	0	0
L_φ	0	0	0	0	-1	2/3	-1/3	-1/3	-1/3	0	0	0
L_z	0	0	1	1	-1	2/3	-1/3	2/3	5/3	0	0	0
M	0	0	0	0	1	0	1	1	1	0	0	0
T	0	0	0	0	0	-2	-3	-3	-3	0	1	0
θ	0	0	0	0	0	-1	-1	-1	-1	1	0	1

As the rank of this matrix is 6, and taking D, L, ρ, c and ΔT_0 as reference variables, the following 6 dimensionless numbers are obtained:

$$\Pi_\theta = \frac{\Delta T}{\Delta T_0}; \qquad \Pi_r = \frac{r}{D}; \qquad \Pi_z = \frac{z}{L}$$

$$\Pi_{k_{rr}} = \frac{k_{rr}t}{\rho c D^2} = \frac{\alpha_{rr}t}{D^2}; \qquad \Pi_{k_{rz}} = \frac{k_{rz}t}{\rho c L D} = \frac{\alpha_{rz}t}{LD}; \qquad \Pi_{k_{zz}} = \frac{k_{zz}t}{\rho c L^2} = \frac{\alpha_{zz}t}{L^2}$$

Thus, the following relationship can be written:

$$\frac{\Delta T}{\Delta T_0} = F\left(\frac{r}{D}, \frac{z}{L}, \frac{\alpha_{rr}t}{D^2}, \frac{\alpha_{rz}t}{LD}, \frac{\alpha_{zz}t}{L^2}\right) \quad (A.10)$$

Assuming isotropy, $\bar{\bar{\alpha}} = \alpha\bar{\bar{I}}$ would be satisfied, i.e. $\alpha_{ij} = \alpha(r,z)\cdot\delta_{ij}$, being δ_{ij} the components of Kronecker delta tensor, and the following numerical, but not dimensional, equalities are verified:

$$\alpha_{rr} = \alpha_{zz} = \alpha(r,z) \quad (A.11)$$

$$\alpha_{rz} = 0 \quad (A.12)$$

Then:

https://doi.org/10.52202/069564-0188

$$[\delta_{rr}] = \frac{[\alpha_{rr}]}{[\alpha]} = \frac{L_r^2 T^{-1}}{L_r^{2/3} L_\varphi^{2/3} L_z^{2/3} T^{-1}} = L_r^{4/3} L_\varphi^{-2/3} L_z^{-2/3} \quad \text{(A.13)}$$

$$[\delta_{zz}] = \frac{[\alpha_{zz}]}{[\alpha]} = \frac{L_z^2 T^{-1}}{L_r^{2/3} L_\varphi^{2/3} L_z^{2/3} T^{-1}} = L_r^{-2/3} L_\varphi^{-2/3} L_z^{4/3} \quad \text{(A.14)}$$

$$\Pi_{k_{rr}} = \frac{\alpha t}{D^2} \cdot \delta_{rr} = \frac{\alpha t}{L^2} \left(\frac{L}{D}\right)^2 \cdot \delta_{rr}; \qquad \Pi_{k_{rz}} = 0; \qquad \Pi_{k_{zz}} = \frac{\alpha t}{L^2} \cdot \delta_{zz}$$

$$\frac{\Delta T}{\Delta T_0} = F\left(\frac{r}{D}, \frac{z}{L}, \frac{\alpha t}{L^2}\left(\frac{L}{D}\right)^2 \cdot \delta_{rr}, \frac{\alpha t}{L^2} \cdot \delta_{zz}\right) \quad \text{(A.15)}$$

which can be rewritten as:

$$\frac{\Delta T}{\Delta T_0} = F\left(\frac{r}{D}, \frac{z}{L}, \frac{\delta_{rr}}{\delta_{zz}}\left(\frac{L}{D}\right)^2, \frac{\alpha t}{L^2} \cdot \delta_{zz}\right) \quad \text{(A.16)}$$

Experimental results can therefore be expressed in terms of $\alpha t/L^2$ and geometrical parameter ratios.

Nomenclature

COP Coefficient of performance

c specific heat capacity, J/(kg·K)

d distance from tube center to probes, m

D tube diameter, m

Fo Fourier number

k thermal conductivity, W/(m·K)

$\{L\}$ dimension of length

L tube length, m

$\{M\}$ dimension of mass

$\{T\}$ dimension of time

T temperature, ºC

T_0 initial probe temperature, ºC

T_∞ steady ground temperature, ºC

r radial distance to tube center, m

t time, s

z depth, m

Greek symbols

α thermal diffusivity, m²/s

α_a apparent thermal diffusivity, m²/s

α_r relative thermal diffusivity, m²/s

α_w water thermal diffusivity, m²/s

δ_{ij} component of Kronecker's delta tensor

ρ density, kg/m³

Π_x dimensional group associated to property x

$\{\theta\}$ dimension of temperature

Subscripts and superscripts

r radial coordinate

φ angular coordinate

z depth coordinate

References

[1] Alva, G., Lin, Y., Fang, G. An overview of thermal energy storage systems. Energy 2018; 144:341-378. DOI: 10.1016/j.energy.2017.12.037.

[2] Alkhalidi,A., Al Khatba, H., Khawaja, M.K. Utilization of Buildings' Foundations for a Seasonal Thermal Energy Storage Medium to Meet Space and Water Heat Demands. International Journal of Photoenergy 2021; 2021:6668079. DOI: 10.1155/2021/6668079.

[3] Barbier, E. Geothermal energy technology and current status: an overview. Renewable and Sustainable Energy Reviews, 6 (1-2), 3-65, 2002. doi.org/10.1016/S1364-0321(02)00002-3.

[4] Reed, A.L., Novelli, A.P., Doran, K.L., Ge, S., Lu, N., McCartney, J.S. Solar district heating with underground thermal energy storage: Pathways to commercial viability in North America. Renewable Energy 2018; 126:1-13. DOI: 10.1016/j.renene.2018.03.019.

[5] Mangold, D., Miedaner,O., Tziggili, E.P., Schmidt, T., Unterberger, M., Zeh,B. Technisch-wirtschaftliche Analyse und Weiterentwicklung der solaren Langzeit-Wärmespeicherung. Schlussbericht zum BMU-Forschungsvorhaben N, 329607, 2012.

[6] Beausoleil-Morrison, I., Kemery, B., Wills, A.D., Meister, C. Design and simulated performance of a solar-thermal system employing seasonal storage for providing the majority of space heating and domestic hot water heating needs to a single-family house in a cold climate. Solar Energy 2019; 191: 57-69. DOI: 10.1016/j.solener.2019.08.034.

[7] Lim, H.S., Ok, J.S., Park, J.S., Lee, S.J., Karng, S.W., Kang, Y.T. Efficiency improvement of energy storage and release by the inlet position control for seasonal thermal energy storage. International Journal of Heat and Mass Transfer 2020; 151:119435. DOI: 10.1016/j.ijheatmasstransfer.2020.119435.

[8] Cruickshank, C.A., Baldwin, C. Sensible thermal energy storage: diurnal and seasonal. In Letcher, T.M.; Ed. Storing Energy. Elsevier; 2016; 291-311. DOI: 10.1016/B978-0-12-803440-8.00015-4.

[9] Arquitectura Bioclimática y Frío Solar (ARFRISOL), Proyecto Singular Estratégico Ref. PS-120000-2005-1. Plan Nacional de Investigación y Desarrollo 2004-2007. Ministerio de Innovación y Ciencia.

[10] Suárez, M.J. Prieto, J.I. Blanco, E. García, D. Tests of an Absorption Cooling Machine at the Gijón Solar Cooling Laboratory. Energies, 13, 3962, 2020. doi:10.3390/en13153962.

[11] Eficiencia energética a través de la Rehabilitación, el Sol y la Geotermia en Asturias. (REHABILITAGEOSOL), RTC-2016-5004-3. Ministerio de Economía, Industria y Competitividad.

[12] Pratt, William K. Digital Image Processing. 4th Ed. Hoboken, NJ, USA: John Wiley & Sons; 2007

[13] Çengel, Y.A.; Ghajar, A.J. Heat and Mass Transfer – Fundamentals & Applications. 5th Ed. New York, USA: McGraw-Hill; 2015.

[14] Ándujar Márquez, J.M., Martínez Bohórquez, M.A., Gómez Melgar, S., Ground Thermal Diffusivity Calculation by Direct Soil Temperature Measurement. Application to very Low Enthalpy Geothermal Energy Systems. Sensors 2016; 16:306. DOI:10.3390/s16030306.

[15] Arkhangelskaya, T., Lukyashchenko, K., Estimating soil thermal diffusivity at different water contents from easily available data on soil texture, bulk density, and organic carbon content. Biosystems Engineering 2018; 168:83-95. DOI: 10.1016/j.biosystemseng.2017.06.011.

[16] Tong, B., Xu, H., Horton, R., Bian, L., Guo, J., Determination of Long-Term Soil Apparent Thermal Diffusivity Using Near-Surface Soil Temperature on the Tibetan Plateau. Remote Sensing 2022; 14:4238. DOI:10.3390/rs14174238

[17] Farouki, O.T. Thermal properties of soils. Hanover, NH, USA: Cold Regions Research and Engineering Lab; 1982.

[18] Dimo, V.N. Physical properties and elements of the heat regime of permafrost meadow-forest soils. Delhi: Indian National Scientific Documentation Centre, Cold Regions Research and Engineering Lab; 1969.

[19] Luikov, A.V. Heat and Mass Transfer in Capillary porous Bodies. New York, USA: Pergamon Press; 1966.

[20] De Vries, D.A. Heat transfer in soils. In De Vries, D.A. Afghan, N.A; Eds. Heat and Mass Transfer In the Biosphere. 1. Transfer Processes in Plant Environment. New York, USA: John Wiley & Sons, Inc., Halsted Press; 1974.

[21] Agencial Estatal de Meteorología de España. Datos abiertos. Available at:<https://www.aemet.es/es/datos_abiertos> [accessed 21/02/2023]

[22] Williams W. On the relation of the dimensions of physical quantities to directions in space. Phil. Mag. 1892;34:234–271. https://doi.org/10.1080/14786449208620315

[23] Huntley HE. Dimensional Analysis. London, UK: McDonald;1952.

[24] Palacios J. Dimensional Analysis. London, UK: McMillan;1964.

[25] Prieto JI, Fano J, Diaz R, Gonzalez MA. Application of discriminated dimensional analysis to the kinematic Stirling engine. Proc. Inst. Mech. Eng. C J. Mech. Eng. Sci. 1994; 208:347–353. https://doi.org/10.1243/PIME_PROC_1994_208_137_02

[26] Madrid CN, Alhama F. Discriminated dimensional analysis of the energy equation: Application to laminar forced convection along a flat plate. International Journal of Thermal Sciences 2005; 44:333–341. https://doi.org/10.1016/j.ijthermalsci.2004.11.008

https://doi.org/10.52202/069564-0188